Optimization of a solution-processed SiO_2 gate insulator by plasma treatment for zinc oxide thin film transistors

*Yesul Jeong,[†] Christopher Pearson,[†] Hyun-Gwan Kim,[‡] Man-Young Park,[‡] Hongdoo Kim,[§] Lee-Mi Do[‖] and Michael C Petty[†]**

[†] School of Engineering and Computing Sciences and Centre for Molecular and Nanoscale Electronics, Durham University, South Road, Durham DH1 3LE, UK.

[‡] Research Center for Nano-Materials, DNF Co. Ltd., Daejeon 306-802, Korea.

[§] Department of Advanced Materials Engineering for Information and Electronics, Kyung Hee University, Yongin 446-701, Korea.

[‖] IT Convergence Technology Research Laboratory, Electronics and Telecommunications Research Institute, Daejeon, Korea.

ABSTRACT

We report on the optimization of the plasma treatment conditions for a solution-processed silicon dioxide gate insulator for application in zinc oxide thin film transistors (TFTs). The SiO_2 layer was formed by spin coating a perhydropolysilazane (PHPS) precursor. This thin film was subsequently thermally annealed, followed by exposure to an oxygen plasma, to form an insulating (leakage current density of ~10^7 A/cm^2) SiO_2 layer. Optimized ZnO TFTs (40 W plasma treatment of the gate insulator for 10 s) possessed a carrier mobility of 3.2 cm^2/Vs, an on/off ratio of ~10^7, a threshold voltage of -1.3 V and a subthreshold swing of 0.2 V/decade. In addition, long-term exposure (150 min) of the pre-annealed PHPS to the oxygen plasma enabled the maximum processing temperature to be reduced from 180 °C to 150 °C. The resulting ZnO TFT exhibited a carrier mobility of 1.3 cm^2/Vs and on/off ratio of ~10^7.

KEYWORDS: solution process, low temperature, solution-processed silicon dioxide, zinc oxide, zinc oxide field-effect transistor, oxygen plasma.

1. INTRODUCTION

High quality gate insulators are key to the commercial success of thin film transistors (TFTs). The dielectric layer has a major influence on the electrical properties of the transistors, for example by controlling the charge carrier density accumulated in the semiconductor channel. Aside from the obvious electrical insulating requirement, there is a focus on developing solution-processible dielectrics that can be formed at low temperatures (e.g. for compatibility with plastic substrates).

Zinc oxide is a popular choice as the semiconductor for TFTs. Morales-Acsta *et al.*[1] have reported sputtered ZnO TFTs with a field effect mobility, μ_{FE}, of 7 cm^2/Vs and an on/off ratio of ~10^5; the device exploited a PMMA-SiO_2 hybrid gate insulator, formed by spin coating on Si followed by annealing at 90 °C. Meena et al.[2] demonstrated PS-b-PMMA/ZnO TFTs utilizing the same processing method as Morales-Acsta *et al*., and achieved μ_{FE} of 2.4 cm^2/Vs, an on/off ratio of ~10^6 and a threshold voltage, $V_{TH,}$ of 2.6V.

There is now an increasing interest in using solution processing to form both the semiconductor and insulating layers in thin film transistors.[3-6] For example, ZnO TFTs using spin coated alumina/polyimide[7] cured at 200 °C and $HfLaO_X$[5] cured at 500 °C have been reported (mobilities of 0.1 cm^2/Vs and 1.6 cm^2/Vs, respectively). In other work, either the processing temperature was too high for flexible substrates or the devices exhibited poor electrical properties.

Silicon dioxide is a well-established gate dielectric, with excellent insulating properties. Unfortunately, it is difficult to exploit this material in solution-processed transistors because a thin film is typically formed using plasma enhanced chemical vapour deposition, physical vapour deposition or sputtering at high temperature. Perhydropolysilazane (PHPS), mainly composed of

Si-N and Si-H, is a precursor for the formation of SiO_2 by solution processing and is an alternative gate material. Matsuo *et al.*[8] first reported that PHPS could be converted to high quality SiO_2 by heat treatment at 450 °C. Consequently, refinement of this reaction has attracted much attention, with the aims of both accelerating the curing process and reducing the curing temperature.[9-11] Bauer *et al.*[9] noted that a moisture-containing atmosphere promotes the hydrolysis and polycondensation reactions needed for the film transformation. In addition, these authors used infrared spectroscopy to demonstrate that a minimum curing temperature of 150 °C is required to form a fully converted SiO_2 film. The action of aqueous ammonia vapour at room temperature for 24 hr on a spin-coated PHPS film was also studied by Kozuka *et al.*[10] This group confirmed that exposure to the ammonia atmosphere partially supported the conversion of PHPS to SiO_2. Recently, solution-processed SiO_2 has been used for sputtered indium-doped ZnO TFTs (IZO TFTs).[12] This study demonstrated that the sputtered IZO semiconductive layer combined with the solution-processed SiO_2 insulator resulted in TFTs with a high mobility of 261.6 cm^2/Vs. However, the devices suffered from a low on/off current ratio and large hysteresis because of the hygroscopic nature of the silazane-derived SiO_2 film. The transistor characteristics were significantly improved by using a spin-coated $LaZrO_x$ film as an additional gate insulator.

In previous work, we have described the use of an oxygen plasma to improve the dielectric properties of PHPS insulator films.[13] It was found that PHPS films cured in a high humidity environment possess a hydrophobic surface, which can be affected by the oxygen plasma. The plasma accelerates the conversion reaction within the PHPS network making it more insulating. Based on these results, we demonstrated a significant improvement in the electrical behavior of ZnO TFTs.

Here we report further details of the conversion of PHPS films to SiO_2 insulators. We also introduce a simple solution-processed approach using only plasma treatment. The changes in the dielectric properties of PHPS following plasma exposure are investigated using atomic force microscopy (AFM), Fourier Transform Infrared (FTIR) spectroscopy and electrical conductivity measurements.

2. EXPERIMENTAL SECTION

Thin Film Fabrication

Solution-processed SiO_2 was formed by the chemical reaction between hydrogen and nitrogen in PHPS solution, as depicted in Fig. 1(a)[9]

$$\left[\mathrm{H_2Si-NH}\right]_n + n\mathrm{H_2O} \xrightarrow{\text{Heat}} n\mathrm{Si(OH)_4} + 2n\mathrm{H_2} + n\mathrm{NH_3} \qquad (1)$$

$$n\mathrm{Si(OH)_4} \xrightarrow{\text{Heat}} n\mathrm{SiO_2} + 2n\mathrm{H_2O}$$

PHPS solution (10% in di-n-butylether (DEB), DPS-10, DNF Co. Ltd) was spin coated on glass slides that had been pre-coated with aluminium (Al) (100 nm thickness) at 3000 rpm followed by pre-annealing in air on a hotplate for 5 min at 150 °C. Pre-annealing at low temperature removes the solvent (boiling point 142 °C). We suggest that this can prevent the generation of defects such as pores or cracks in the film, which are caused by sudden evaporation during curing. These films were placed in an Espec SH-641 bench-top type temperature and humidity chamber (75 °C, 75%), and cured on a hotplate for 1 hr at 180 °C, which were found to be the minimum time and temperature for formation of the SiO_2 network (Fig. S2 and Fig. S3). Immediately after annealing, the films were exposed to an oxygen plasma (Yield Engineering

System Inc., YES-R3) for 10 sec at RF powers of 20, 40 and 80 W. To produce PHPS films without the curing stage, the pre-annealed film was exposed to the plasma for 150 min at 40 W.

Throughout this paper, the following nomenclature is used to identify PHPS layers that had been subjected to the various processing steps:

PS – as-deposited PHPS

APS – pre-annealed PHPS

CAPS – cured and pre-annealed PHPS

OPS – oxygen plasma-treated as-deposited PHPS

OAPS – oxygen plasma-treated and pre-annealed PHPS

OCAPS – oxygen plasma-treated, cured and pre-annealed PHPS

Transistor fabrication and characterization

Solution-processed PHPS/ZnO TFTs were fabricated on clean glass substrates. The TFT structure used in this study is shown in Fig. 1(b). CAPS, OCAPS, OPS and OAPS films were formed onto pre-patterned Al gate electrodes[14-17] (100 nm thick) fabricated by thermal evaporation through a shadow mask. Zinc oxide solution,[18] composed of 0.081 g of ZnO (Sigma–Aldrich, ≥99.9%) in 9.8 g aqueous ammonia solution, was spin-coated (3000 rpm, 30 sec) on the gate insulator to a thickness of approximately 20 nm and then annealed at 140 °C for 30 min. Conductivity through the ZnO films was investigated by tunnelling atomic force microscopy (TUNA), as shown in Fig. S1. Finally, 100 nm thick Al source/drain (S/D) electrodes[7,19-22] were deposited by thermal evaporation onto the semiconducting layer through a shadow mask, creating transistors with a channel width (W) and length (L) of 1000 μm and 50 μm, respectively.

The contact angles and morphologies of the insulator films were measured using a water drop contact angle system and a Digital Instruments Nanoman II AFM, respectively. FTIR spectra of the gate dielectric films before and after the plasma treatment were obtained using a Nicolet Nexus spectrometer with a HgCdTe crystal detector. The measurements were made in reflection mode (angle of incidence 80°). The background spectrum was recorded by collecting 128 scans over the range 400 cm^{-1} to 4000 cm^{-1} using an Al coated glass slide. The current density, *J*, versus electric field, *E*, of Al/gate insulator/Al structures after plasma treatment was measured using a Keithley 2400 SourceMeter. Characteristics of transistor devices were monitored using a Keithley 4140B pA meter/DC voltage source. The capacitance versus frequency characteristics of insulator films deposited onto Au electrodes and with evaporated Al top contacts were measured using an HP 4192A LF Impedance Analyzer over the frequency range 1 kHz to 1MHz. Electrical measurements were undertaken in air and in the dark, without any encapsulation.

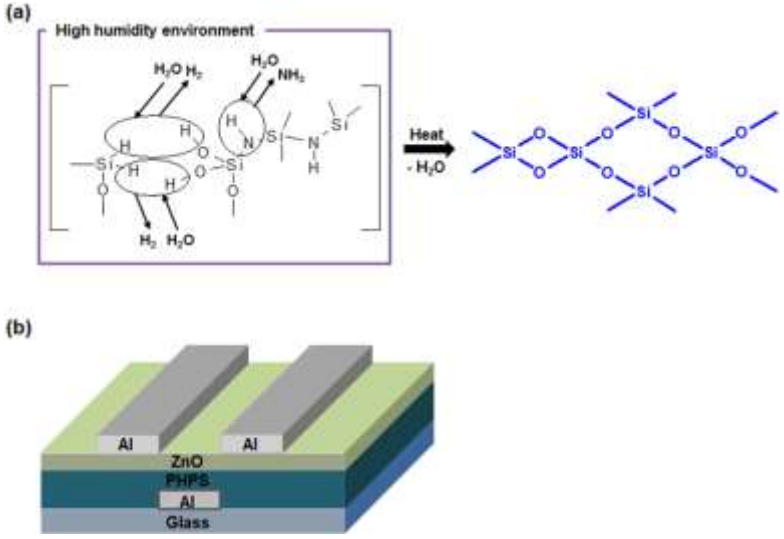

Figure 1. (a) Conversion of PHPS into SiO_2 in a high humidity environment. (b) Architecture of PHPS/ZnO TFTs.

3. RESULTS AND DISCUSSION

Morphology and chemistry of the gate insulator

The contact angles on CAPS and after plasma treatment (OCAPS) at 20, 40 and 80 W for 10 sec are shown in Fig. 2. The value for CAPS was 78°, which is indicative of a hydrophobic surface. However, this was reduced to less than 1° after the oxygen plasma treatment at 80 W. This is certainly due to the production of hydrophilic groups on the CAPS surface by binding of oxygen radicals from the plasma. The minimum plasma RF power to change the surface from hydrophobic to hydrophilic was 40 W.

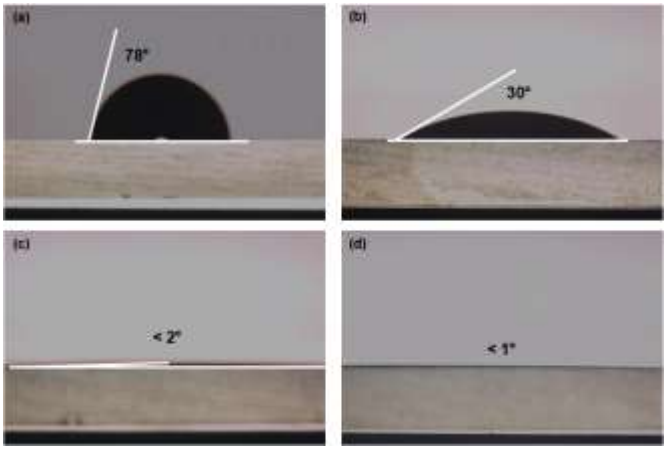

Figure 2. The contact angles for water measured on (a) CAPS and OCAPS with plasma treatment at (b) 20, (c) 40 and (d) 80 W for 10 sec.

Figure 3(a)-(d) shows tapping mode AFM topography images (not normalized) of CAPS and OACPS films on Al as a function of the plasma RF power. The films are all similar, with no evidence of roughness or cracking, suggesting that, irrespective of the power used, the plasma treatment does not induce surface damage. AFM images of ZnO spin-coated onto CAPS and 20, 40 and 80 W OCAPS are shown in Fig. 3 (e)-(h). As predicted by the contact angle

measurements, ZnO films on CAPS possess very poor surface uniformity (Fig. 3(e)). However, well-formed grains are evident for ZnO films deposited on OCAPS processed at both 40 W and 80 W, Fig. 3(g) and 3(h). No definite conclusions can be drawn from the AFM image of the 20W OCAPS, Fig. 3(f)). Either the ZnO has not deposited or its grain structure is relatively fine. These results demonstrate that plasma treatment using an optimized power enables the formation of a completely uniform semiconductor film.

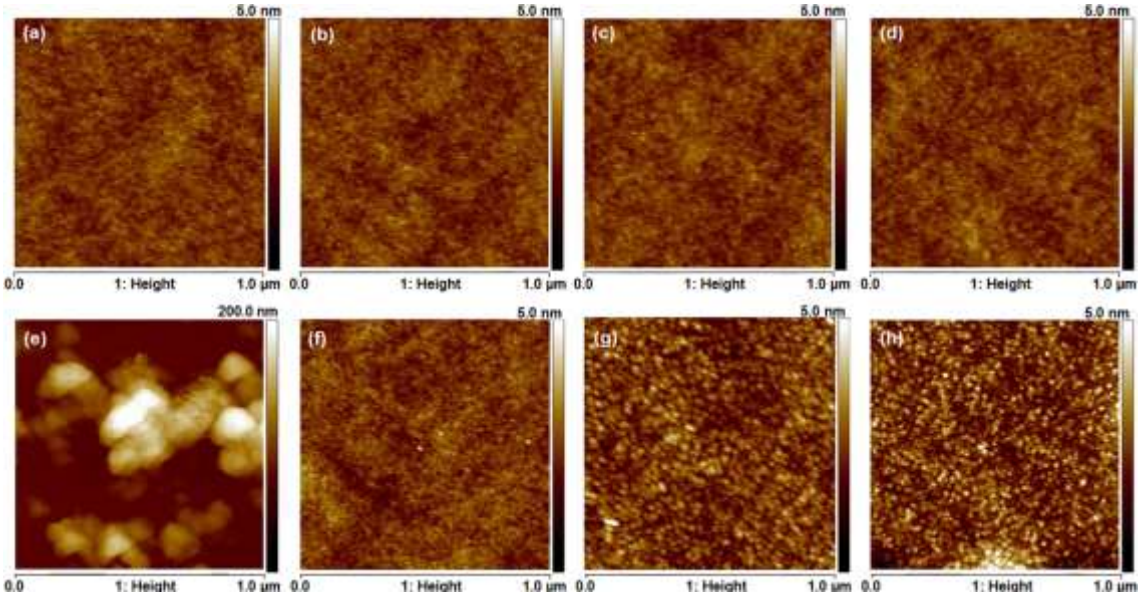

Figure 3. AFM topography images of (a) CAPS and (b) 20, (c) 40, and (d) 80 W OCAPS films on Al. AFM topography images of ZnO thin films spin-coated onto (e) CAPS/Al and (f) 20, (g) 40, and (h) 80 W OCAPS/Al.

Infrared spectra are shown in Fig. 4 while Table 1 provides the IR peak assignments.[8, 23-26] It has previously been shown that above 300 °C, the hydrolysis of Si-N and Si-H bonds leads to the formation of a SiO_2 network.[8, 23-24] In the case of CAPS, the main absorption bands are observed at approximately 1180 cm^{-1} and 3360 cm^{-1} and correspond to the bend and stretch modes of N-H, respectively. In addition, bands at 920 cm^{-1}, 840 cm^{-1} and 2160 cm^{-1} indicate the presence of Si-

N and Si-H bonds in the CAPS film. These results imply that a SiO_2 network is only partially formed after the curing process, probably because of the relatively low curing temperature. However, the number of unreacted groups, such as N-H and Si-H, in the CAPS film gradually decreases with an increase in the plasma power. It is evident that the IR absorbance spectrum of the film treated at 40 W shows only two main absorption peaks, at 460 cm^{-1} and 1060 cm^{-1}, relating to the Si-O bond, with shoulders at 800 cm^{-1} and 1170 cm^{-1} (Si-O-Si stretching). We suggest that the partially converted PHPS film is completely changed to SiO_2 as a result of the removal of unreacted groups by the oxygen plasma.

When the plasma treatment power was increased from 40 W to 80 W, a new broad peak appeared at 3600 cm^{-1}; this was assigned to a Si-OH stretch and was only observed for the CAPS film that was subjected to plasma treatment at 80 W. This indicates that this peak is not related to dangling bonds that were unavoidably generated during the CAPS film formation. An increase in the RF power leads to an increase in both the density and energy of the radicals in the plasma. We propose that the new feature in the FTIR spectrum for the 80 W OCAPS is related to a reaction between the residual oxygen radicals on the OCAPS surface and the water in the surrounding environment[27-28]

$$O\cdot + H_2O \rightarrow \cdot OH + \cdot OH \qquad (2)$$

The optimum RF power needed to provide a complete SiO_2 network appears to be 40 W.

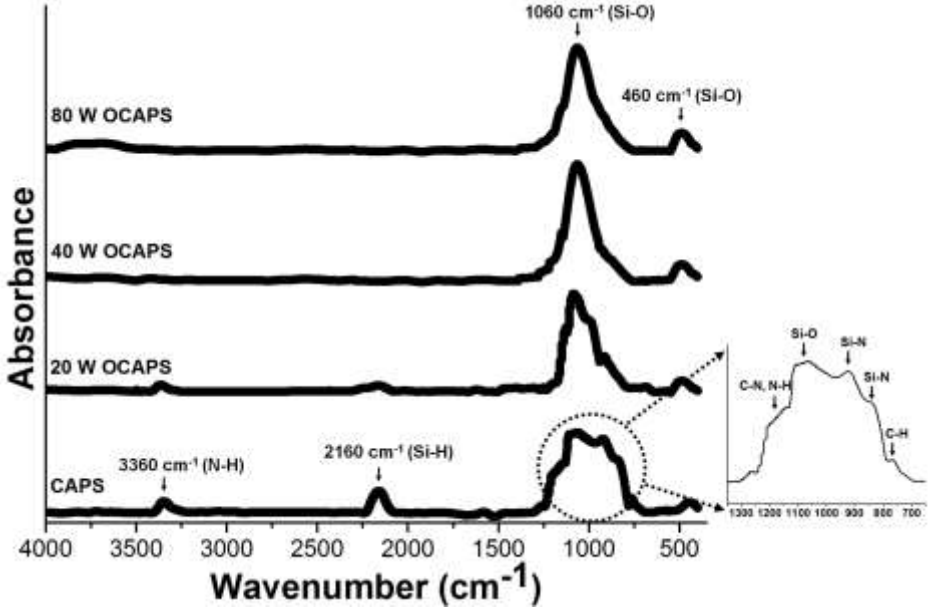

Figure 4. FTIR spectra measured for OCAPS films as a function of the plasma RF power.

Group vibration	Wavenumber (cm^{-1})
Si-O rock	460
C-H bend	680-860
Si-N stretch in Si-N-Si	920,840
Si-O stretch	1060
Si-O-Si stretch	800, 1170
C-N stretch	1000-1250
N-H bend	1180
Si-H stretch	2160
N-H stretch	3360
Si-OH stretch	3600

Table 1. IR peak assignments.

Electrical characteristics of the gate insulator

Figure 5 shows the current density versus electric field through Al/insulator/Al structures with thicknesses in the range 150-160 nm and for a contact area of 0.8×10^{-2} cm^2. The bias was swept at a scan rate of 2.0×10^{-2} V/s over the range 0V >±20V > 0V. No reliable data were obtained for current densities less than about 10^{-10} A/cm^2 as the measured currents became comparable to the offset in our instrumentation system. For the CAPS film (Fig. 5(a)), a current density of 1.0×10^{-5} A/cm^2 at 1 MV/cm was measured, with hysteresis in both the forward and reverse scans. The 20 W OCAPS layer (Fig. 5(b)) shows slightly smaller current density with reduced hysteresis. In contrast, the 40 W OCAPS film (Fig. 5(c)) exhibits a current density approximately two order of magnitude lower, i.e. 7.5×10^{-7} A/cm^2 at 1 MV/cm, which is

comparable to the conductivity of this insulator reported by others.[3-4, 29] For this sample, the hysteresis in the *J vs E* characteristic is significantly reduced. As the plasma treatment power was increased to 80 W, a similar current density to that exhibited for 40 W OCAPS is noted (Fig. 5(d)), but with increased hysteresis. It has been demonstrated that precursor groups (Si-N, Si-H) remaining after conversion and hydroxyl groups on the SiO_2 surface lead to the presence of hysteresis.[30-33] On the basis of the IR results shown in Fig. 4, we suggest that the hysteresis in the *J vs E* curves for CAPS and 20 W OCAPS is attributed to incomplete reaction of the PHPS precursor, and that hydroxyl groups generated after plasma treatment introduce hysteresis for 80 W OCAPS films.

The dielectric constants for CAPS were estimated to be 5.8 and 4.7 at 1 kHz and 1 MHz, respectively; in the case of the 40 W OCAPS film, the corresponding values were 5.1 at 1 kHz and 4.7 at 1 MHz (Fig. S4). These figures are somewhat larger than those expected for SiO_2; however it should be noted that (i) the dielectric constant for SiO_2 varies with processing conditions[34] and (ii) the PHPS films may contain additional polar groups that can contribute to the measured permittivity.

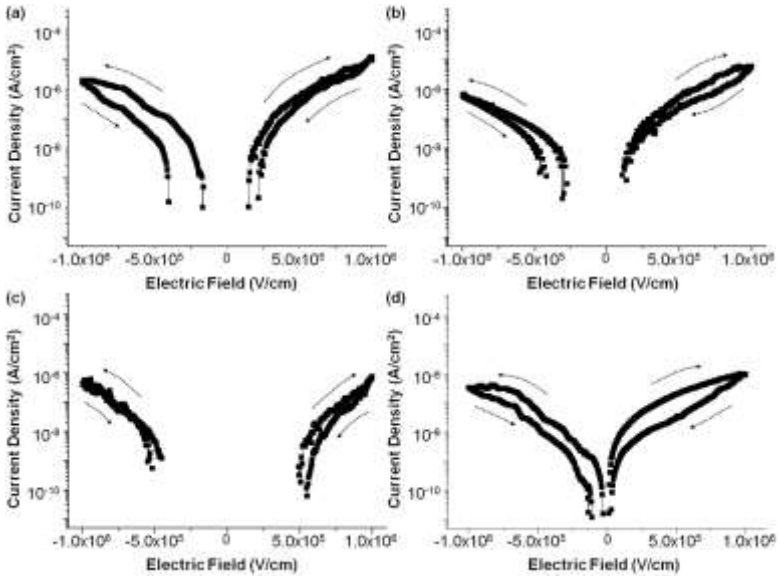

Figure 5. Current density versus electric field characteristics of Al/insulator/Al structures: (a) reference CAPS and (b) 20 W, (c) 40 W and (d) 80 W OCAPS films. Film thicknesses 150-160 nm. Data are shown for both forward and reverse voltage scans.

We have attempted to fit our data to electrical conductivity models that might be expected to operate under the high field regime for silicon dioxide thin films, specifically Schottky emission and Poole-Frenkel conduction.[35] These processes both result from the reduction of Coulombic potential barriers by an applied electric field. Whilst Schottky emission is an electrode-limited conduction process, the Poole-Frenkel effect is a bulk-limited mechanism. The current densities may be expressed as[35,36]

$$J_S = T^2 \exp\left[\frac{q}{kT}\sqrt{\frac{qE}{4\pi\varepsilon_0\varepsilon}} - \frac{q\Phi_S}{kT}\right] \quad \text{for Schottky emission,} \qquad (3)$$

$$J_{PF} = E \exp\left[\frac{q}{kT}\sqrt{\frac{qE}{\pi\varepsilon_0\varepsilon}} - \frac{q\Phi_{PF}}{kT}\right] \quad \text{for Poole-Frenkel emission,} \qquad (4)$$

where ε, Φ_S and Φ_{PF} are the relative permittivity of the insulating layer, and the barrier heights for trapped electrons in the case of Schottky emission and Poole-Frenkel emission, respectively. The dominant mechanism can be determined by demonstrating a linear relationship between *ln(J) vs* $E^{1/2}$ for Schottky emission and *ln(J/E) vs* $E^{1/2}$ for Poole-Frenkel conduction. Figure 6 depicts Schottky and Poole-Frenkel plots for CAPS and 40 W OCAPS. Although improved fits for both conduction processes are obtained for films that had been subjected to the plasma processing, the plots do not reveal convincing straight lines over the entire range of electric field used. We have evaluated the permittivity of the CAPS and 40 W OCAPS gate insulators from the slopes of the best straight line fits to the Schottky and Poole-Frenkel equations (Eqns. (4) and (5)). In both the forward and reverse scans, permittivities of the order 10^{-2} were obtained, suggesting that other electrical processes are likely to be contributing to the electrical conductivity of these particular insulators. This is further discussed in the later section dealing with OAPS layers.

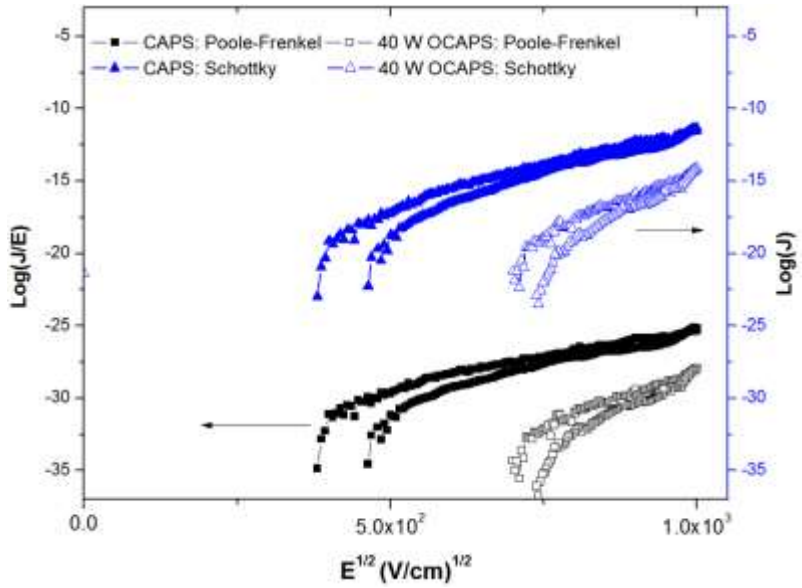

Figure 6. Schottky (*ln(J) vs* $E^{1/2}$) and Poole-Frenkel (*ln(J/E) vs* $E^{1/2}$) plots for CAPS and 40 W OCAPS. Data are shown for forward and reverse voltage scans.

Transistor characterization

Figure 7(a) shows the transfer characteristics, drain-source current, I_{DS}, versus gate voltage, V_G, for TFTs having CAPS gate insulators exposed to different oxygen RF plasma powers. All devices were measured at V_{DS} = 50 V, which is in the saturation region of the output curve shown later in Fig. 8; the characteristics for the linear region, V_{DS} = 10 V, are provided in Fig. S5. The field effect mobility and threshold voltage in the saturation region of the devices were extracted from the linear fits of the following expression

$$I_{DS}^{1/2} = \left(\frac{WC_i\mu_{FE}}{2L}\right)^{\frac{1}{2}}(V_G - V_{TH}) \qquad (5)$$

where C_i is the capacitance per unit area of the insulator layer, as shown in Fig. 7(b) for the CAPS/ZnO reference TFT and that exposed to the 40 W plasma (40W OCAPS/ZnO). The subthreshold swing (*SS*) was calculated from the linear region of the forward scan using

$$SS = \frac{dV_G}{d(\log I_{DS})} \qquad (6)$$

SS is defined in this study as the value of V_G required to increase I_{DS} by a factor of ten (from 10^{-10} to 10^{-9} A).

The detailed electrical properties of these ZnO TFTs are summarized in Table 2; all values are calculated from the forward scan of the transfer curve. The TFTs appear to be partly turned on at negative gate bias, presumably by holes generated below the gate insulator or via leakage paths. This effect is evident in other reports on ZnO transistors.[4,37-39] The on/off ratios given in Table 2 are the ratios of the I_{DS} magnitudes at gate biases of 80 V and 0 V. It is clear that the ZnO TFT

using CAPS exhibits relatively poor transistor characteristics (low mobility), while the plasma treatment leads to enhancement of the electrical properties. The transfer characteristics measured for the 20 W OCAPS layer confirm the presence of the ZnO semiconductive layer (see earlier discussion of the AFM images in Fig. 3). The calculated leakage currents of CAPS and 40 W OCAPS films measured at 1 MV/cm shown in Fig. 5 are ~10^{-9} A and ~10^{-11} A, respectively; the electric field corresponds to $V_G \approx 15$ V. The inferior electrical properties of CAPS/ZnO TFTs are attributed to the non-uniform nature of the ZnO semiconductor layer on the insulator caused by the hydrophobic nature of CAPS (Figs. 2 and 3) and to the presence of unconverted PHPS precursor in the film (Fig. 4).

Zinc oxide TFTs using 40 W and 80 W OCAPS reveal improved transistor performance with a μ_{FE} of 3.2 cm^2/Vs, on/off ratio of ~10^7, V_{TH} of -1.3 and -1.5 V, and *SS* of 0.2 and 0.6 V/decade, respectively. This trend is consistent with the decreasing current density with increasing plasma power, evident in Fig. 5. Larger hysteresis is observed for ZnO TFTs fabricated with 80 W OCAPS. This is probably related to the hydroxyl groups on the insulator surface, identified by IR measurements, acting as trap sites.

Further insight into the device behavior can be provided by calculation of the trap density, D_{it}, from the *SS* value, according to the following equation[40]

$$D_{it} = \left(\frac{qSS\log(e)}{kT} - 1\right) \cdot \frac{C_i}{q} \qquad (7)$$

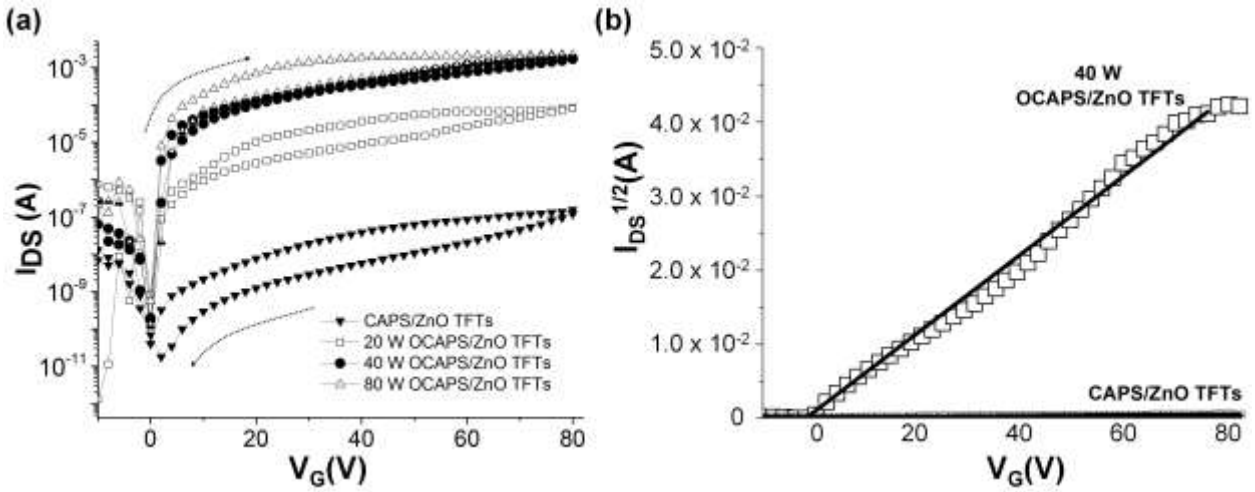

Figure 7. (a) Transfer characteristics of CAPS/ZnO TFTs, measured at V_{DS} = 50 V, with various plasma treatment powers. Data are shown for forward and reverse voltage scans. (b) Plots of $I_{DS}^{1/2}$ versus V_G for CAPS/ZnO and 40 W OCAPS/ZnO TFTs (forward scans). The full lines are best straight line fits to the data points.

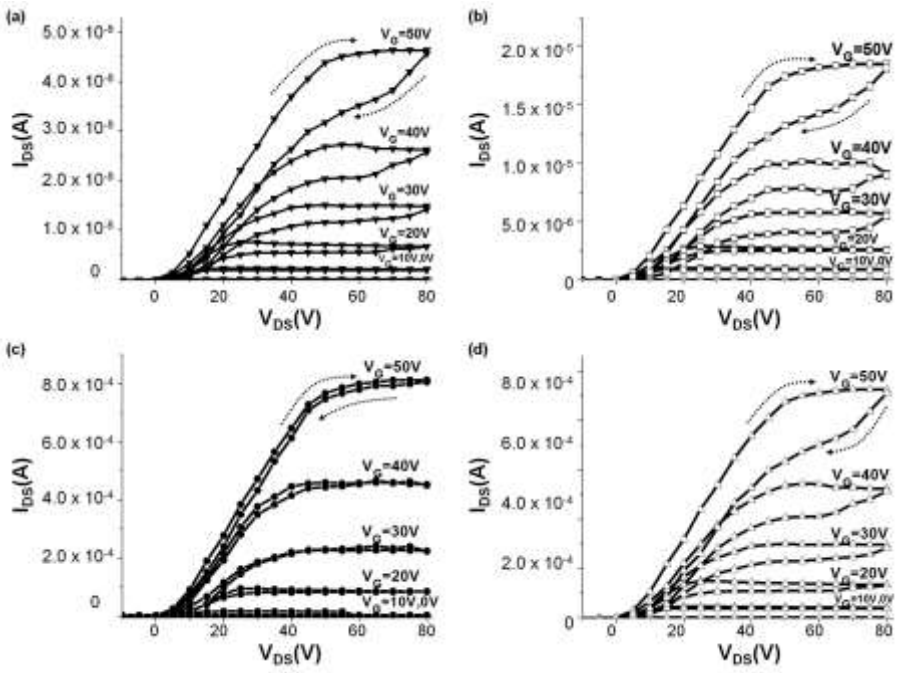

Figure 8. Output characteristics (I_{DS} - V_{DS} curves) of (a) CAPS and (b) 20 W, (c) 40 W, and (d) 80 W OCAPS/ZnO TFTs. Data for each V_G value are shown for forward and reverse V_{DS} scans.

It is evident from Table 2 that the D_{it} value is minimized for the 40 W OCAPS/ZnO TFT, at a figure of 3.5 x 10^{11} /eVcm^2.

Figure 8 shows the output characteristics, I_{DS}, versus drain-to source voltage, V_{DS}, for TFTs treated with different oxygen plasma powers. The gate voltage was measured in the range 0 to 50 V in steps of 10 V. Typical n-channel electrical properties are observed. Although all devices showed good current saturation, devices using CAPS, 20 W and 80 W OCAPS exhibit hysteresis, due to the presence of traps on the surface of the SiO_2. The current at low I_{DS}, generally influenced by the contact resistance(s) between the semiconductor and S/D,[41] slowly increased and exhibited non-linear behavior. This can be explained by the (unavoidably generated) natural oxide on Al following exposure to air.[42] This thin oxide layer provides a higher work function than pure Al, leading to a poor contact between the ZnO and the source and drain electrodes. In further work, it might be possible to reduce this effect by using a suitable plasma treatment, although a different TFT architecture would be needed.[42,43] The negative values of V_{TH} in Table 2 suggest that our transistors may operate in depletion mode. This has been noted for oxide TFTs and is related to fixed charges in the insulator, interface and semiconductor regions.[44-46]

Overall, the manipulation of the SiO_2 gate insulator network by plasma treatment resulted in improved transistor performance; the ZnO devices processed with 40 W RF power exhibited the optimum TFT device characteristics.

	μ_{FE} (cm^2/Vs)	on/off ratio	V_{TH} (V)	SS (V/decade)	D_{it} (/eVcm^2)
CAPS	1×10^{-2}	$\sim 10^2$	-1.2	5.5	1.1×10^{13}
20 W OCAPS	8×10^{-2}	$\sim 10^4$	-1.3	0.7	1.4×10^{12}
40 W OCAPS	3.2	$\sim 10^7$	-1.3	0.2	3.5×10^{11}
80 W OCAPS	3.2	$\sim 10^7$	-1.5	0.6	1.3×10^{12}

Table 2. Summary of the electrical properties of ZnO TFTs.

Reduced processing temperature

To reduce further the processing temperature of our TFTs, we have investigated the behavior of devices that had only been subjected to pre-annealing and plasma processing. Figure 9 shows the FTIR spectrum of OAPS after oxygen plasma treatment at 40 W for 150 min (note the much longer plasma processing time used in this experiment). The differences in the IR absorption peaks of APS as a function of plasma treatment time are revealed in more detail in Fig. S6. The IR absorbance spectra of APS exhibit relatively high intensity hydrogen and nitrogen peaks from the PHPS network, which disappear after plasma treatment for 150 min. For example, the APS film possesses a clear absorption maximum at 920 cm^{-1} (Si-H stretching) with shoulders at 1186 cm^{-1} and 840 cm^{-1} indicating N-H bonding and Si-N stretching in Si-N-Si, respectively. In addition, small absorption peaks from N-H stretching and Si-H stretching are observed at 3360 cm^{-1} and 2160 cm^{-1}, respectively. However, the APS film was totally converted to SiO_2 after

extended oxygen plasma treatment, confirmed by the existence of only well-defined absorptions related to Si-O bonding at 460 cm^{-1} (Si-O rocking) and 1060 cm^{-1} (Si-O stretching). These results indicate that an extended oxygen plasma treatment (instead of curing at 180 °C in a high humidity environment) is an effective method for the complete conversion of PHPS into SiO_2.

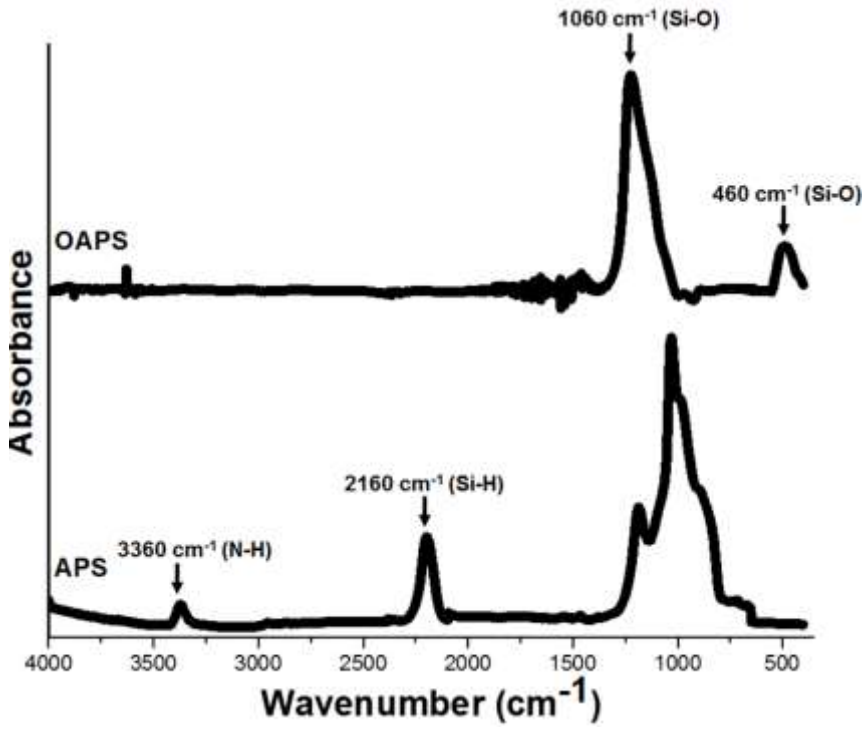

Figure 9. FTIR spectra of an APS film and an OAPS film after an oxygen plasma treatment at 40 W for 150 min.

Figure 10 depicts the *J-E* properties of OAPS measured using an Al/OAPS/Al structure. Interestingly, the current density of 7.2 x 10^{-7} A/cm^2 at 1 MV/cm for APS with plasma treatment for 150 min is lower than that observed for 40 W OCAPS (Fig. 5). To determine the dominant conduction mechanism in OAPS, the *J-E* plots (positive bias) of Fig. 10 are re-plotted as *ln(J/E)* as a function of $E^{1/2}$ for Poole-Frenkel emission and as *ln(J) vs* $E^{1/2}$ for Schottky emission. The results are presented in Fig. 11, which reveals significantly improved straight line fits in

comparison with Fig. 6, particularly for the Poole-Frenkel plot. In this case, the value of the insulator permittivity obtained from the slope of the line is 3.3, in reasonable agreement (i.e. within experimental error) with the extracted dielectric constant from this study (Fig S4) and vacuum-processed SiO_2,[39] suggesting that the dominant conduction mechanism of OAPS is the Poole-Frenkel effect. (The permittivity value obtained from the best fit to the Schottky plot was 0.17.)

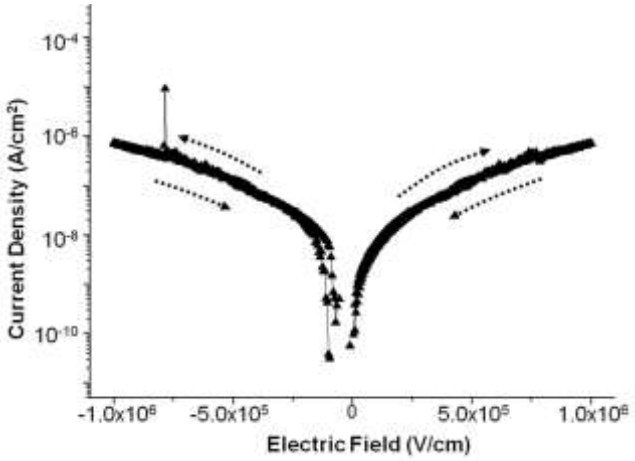

Figure 10. Current density versus electric field for OAPS with plasma treatment for 150 min. Data are shown for forward and reverse voltage scans.

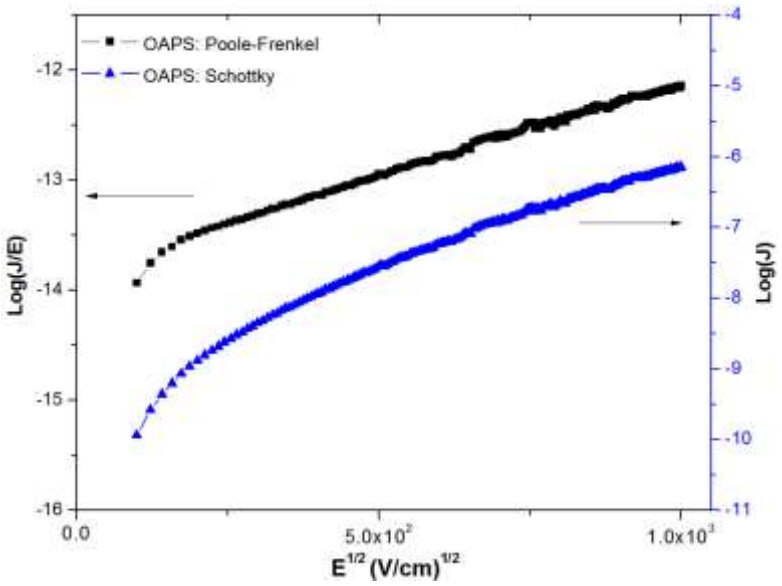

Figure 11. Schottky (*ln(J) vs* $E^{1/2}$) and Poole-Frenkel (*ln(J/E) vs* $E^{1/2}$) plots for OAPS (plasma treatment for 150 min). Data are shown for forward voltage scan.

If Poole-Frenkel conductivity is the dominant process in our OAPS layers, then it is curious that this conductivity mechanism does not seem so clearly established in the OCAPS layers (Fig. 6). Although the infrared experiments suggest that the 40 W OCAPS film has been fully converted to SiO_2, it is plausible that some surface states remain. These will trap charge and influence the distribution of the electric field across the thin film. The extended plasma processing (150 min) needed to convert the APS film to SiO_2 leads to a complete elimination of these surface states and results in an electrical conduction process (Poole-Frenkel) that is dominated by bulk traps. For example, Jeong *et al.*[47] have reported on Poole-Frenkel conductivity in siloxane organic-inorganic gate insulators and suggested that injected electrons are trapped at silanol groups in the insulator. More detailed studies (e.g. over an extended temperature range) are clearly needed to elucidate the nature of the surface and bulk states in our thin films as a function of the film processing conditions.

The transfer characteristics (I_{DS} *vs* V_G) measured at V_{DS}= 50 V and output characteristics (I_{DS} *vs* V_{DS}) measured at several V_G values in the range of 0 to 50 V in steps of 10 V obtained from an OAPS TFT are shown in Fig. 12. The device showed good current saturation in the output characteristics with relatively little hysteresis. Promising transistor performance was observed with a μ_{FE} of 1.3 cm^2/Vs, on/off ratio of ~10^7, *SS* of 1.65 V/decade, V_{TH} of -1.6 V and D_{it} of 3.4 x 10^{12} /eVcm^2. The carrier mobility of this TFT is somewhat lower than that obtained from ZnO TFTs using 40 W and 80 W OCAPS. However, our preliminary results indicate that simple processing at a relatively low fabrication temperature is a viable route to manufacture ZnO/SiO_2 thin film transistors.

For completeness, we have also taken the opportunity to investigate the changes of PS using the plasma treatment for 150 min at 40 W (i.e. the pre-annealing device processing step at 150 °C is also eliminated). The results show that the PHPS precursor is fully formed into a SiO_2 network, evident by possessing the FTIR absorptions related to only Si-O bonding (Fig. S7). In addition, a current density of 3.6 x 10^{-6} A/cm^2 at 1 MV/cm was measured with significant hysteresis (Fig. S8). However, reliable transistor operation could not be achieved using only the plasma processing step.

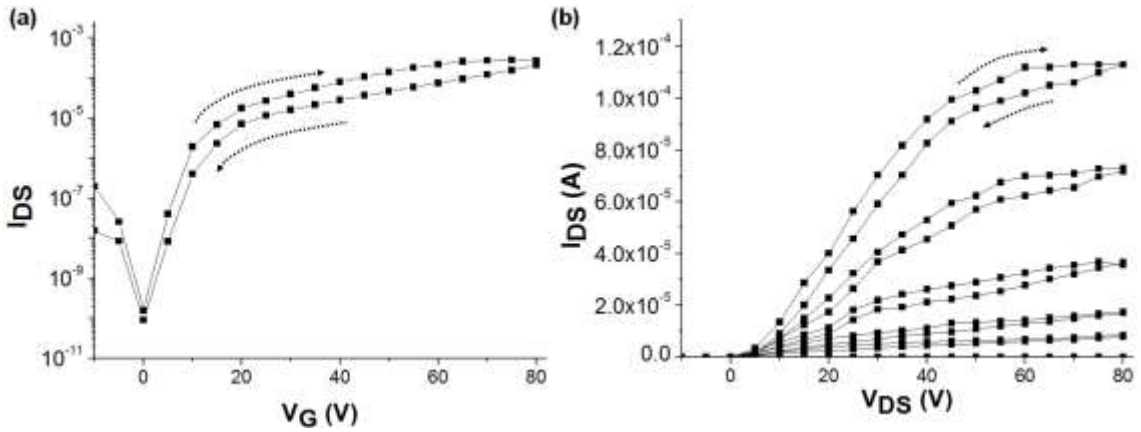

Figure 12. (a) Transfer and (b) output characteristics of a ZnO TFT using APS with plasma treatment for 150 min as the gate insulator. Data are shown for forward and reverse voltage scans.

4. CONCLUSION

This study explores the effect of oxygen plasma treatment of spin-coated perhydropolysilizane gate dielectric layers on the performance of zinc oxide thin film transistors. The surface wettability of pre-annealed (150 °C) and cured (180 °C in high humidity) thin films was changed from hydrophobic to hydrophilic by the plasma treatment. This leads to good adhesion between ZnO and the insulator. Infrared spectroscopic studies confirmed that the plasma treatment accelerated the hydrolysis and polycondensation reactions. This produced a marked improvement in the insulating properties of the resulting silicon dioxide layer. Optimum transistor performance was achieved using an RF plasma power of 40 W for 10 s. These devices possessed a field effect mobility of 3.2 cm^2/Vs, on/off ratio of ~10^7 and a threshold voltage of -1.4 V. The device fabrication temperature could be further reduced, to 150 °C, by elimination of the curing stage and extended exposure of the pre-annealed perhydropolysilizane film to the oxygen plasma.

ASSOCIATED CONTENT

Supporting Information.

Contact mode AFM height and TUNA images of a ZnO film, FTIR absorption of the CAPS layer according to curing temperature and time, capacitance per unit area for CAPS and 40W OCAPS films, transfer characteristics in the linear region for ZnO TFTs using CAPS and OCAPS films with various plasma treatment powers, FTIR spectra of APS, OAPS PS and OPS films, and current density versus electric field for Al/OPS/Al structure. This material is available free of charge via the Internet at http://pubs.acs.org.

AUTHOR INFORMATION

Corresponding Author

*E-mail: m.c.petty@durham.ac.uk

Present Addresses

School of Engineering and Computing Sciences and Centre for Molecular and Nanoscale Electronics, Durham University, South Road, Durham DH1 3LE, UK.

ACKNOWLEDGMENT

This work was supported by the Industrial Strategic Technology Development Program (10041808, Synthesis of Oxide Semiconductor and Insulator Ink Materials and Process Development for Printed Backplane of Flexible Displays Processed Below 150°C) funded by the Ministry of Knowledge Economy (MKE, Korea).

REFERENCES

(1) Morales-Acosta, M. D.; Quevedo-López, M. A.; Ramírez-Bon, R. PMMA–SiO_2 Hybrid Films as Gate Dielectric for ZnO Based Thin-Film Transistors. *Mater. Chem. Phys.* **2014**, 146, 380–388.

(2) Meena, J. S.; Chu, M.-C.; Singh, R.; Wu, C.-S.; Chand, U.; You, H.-C.; Liu, P.-T.; Shieh, H.-P. D.; Ko, F.-H. Polystyrene-Block-Poly(methylmethacrylate) Composite Material Film as a Gate Dielectric for Plastic Thin-Film Transistor Applications. *R. Soc. Chem. Adv.* **2014**, 4, 18493–18502.

(3) Jung, Y.; Jun, T.; Kim, A.; Song, K.; Yeo, T. H.; Moon, J. Direct Photopatternable Organic–Inorganic Hybrid Gate Dielectric for Solution-processed Flexible ZnO Thin Film Transistors. *J. Mater. Chem.* **2011**, 21, 11879–11885.

(4) Kim, K.; Lee, E.; Kim, J.; Park, S. Y.; Lim, K.-H.; Shin, C.; Kim, Y. S. Interface Engineering for Suppression of Flat-Band Voltage Shift in a Solution-Processed ZnO/Polymer Dielectric Thin Film Transistor. *J. Phys. Chem. C* **2013**, 1, 7742–7747.

(5) Ko, J.; Kim, J.; Park, S. Y.; Lee, E.; Kim, K.; Lim, K.-H.; Kim, Y. S. Solution-Processed Amorphous Hafnium-lanthanum Oxide Gate Insulator for Oxide Thin-Film Transistors. *J. Phys. Chem. C* **2014**, 2, 1050–1056.

(6) Hwang, B.-U.; Kim, D.-I.; Cho, S.-W.; Yun, M.-G.; Kim, H. J.; Kim, Y. J.; Cho, H.-K.; Lee, N.-E. Role of Ultrathin Al_2O_3 Layer in Organic/Inorganic Hybrid Gate Dielectrics for Flexibility Improvement of InGaZnO Thin Film Transistors. *Org. Electron.* **2014**, 15, 1458–1464.

(7) Yoo, S.; Yoon, J.-Y.; Ryu, J.; Kim, Y. H.; Ka, J.-W.; Yi, M. H.; Jang, K.-S. Low-Temperature-Annealed Alumina/Polyimide Gate Insulators for Solution-processed ZnO Thin-Film Transistors. *Appl. Surf. Sci.* **2014**, 313, 382–388.

(8) Matsuo, H.; Yamada, K. Topics on Coating. Ceramic Coating Capable Low-Temperature Formation Using Inorganic Polysilazane. *Convertech* **1995**, 23, 25–29.

(9) Bauer, F.; Decker, U.; Dierdorf, A.; Ernst, H.; Heller, R.; Liebe, H.; Mehnert, R. Preparation of Moisture Curable Polysilazane Coatings. *Prog. Org. Coat.* **2005**, 53, 183–190.

(10) Kozuka, H.; Fujita, M.; Tamoto, S. Polysilazane as the Source of Silica: the Formation of Dense Silica Coatings at Room Temperature and the New Route to Organic–Inorganic Hybrids. *J. Sol-Gel Sci. Technol.* **2008**, 48, 148–155.

(11) Tomoko K.; Eisuke T.; Kozuka, H. Preparation of Hot Water-Resistant Silica Thin Films from Polysilazane Solution at Room Temperature. *J. Sol-Gel Sci. Technol.* **2004**, 31, 257–261.

(12) Je, S. Y.; Son, B.-G.; Kim, H.-G.; Park, M.-Y.; Do, L.-M.; Choi. R.; Jeong. J. K. Solution-Processable $LaZrO_x/SiO_2$ Gate Dielectric at Low Temperature of 180 °C for High-Performance Metal Oxide Field-Effect Transistors. *ACS Appl. Mater. Interfaces*, **2014**, 6, 8693–8703.

(13) Jeong, J.; Pearson, C.; Kim, H. -G.; Park, M. -Y.; Kim, H.; Do, L. -M.; Petty, M. C. Solution-Processed SiO_2 Gate Insulator Formed at Low Temperature for Zinc Oxide Thin-Film Transistors. *R. Soc. Chem. Adv.* **2015**, 5, 36083–36087.

(14) Noh, S. H.; Choi, W.; Oh, M. S.; Hwang, D. K.; Lee, K.; Im, S.; Jang, S.; Kim, E. ZnO-Based Nonvolatile Memory Thin-Film Transistors with Polymer Dielectric/ferroelectric Double Gate Insulators, *Appl. Phys. Lett.* **2007**, 90, 253504.

(15) Kwon, Y.; Li. Y.; Heo, Y. W.; Jones, M.; Holloway, P. H.; Norton, D. P., Park, Z. V.; Li, S. Enhancement-Mode Thin-Film Field-Effect Transistor Using Phosphorus-doped (Zn,Mg)O Channel, *Appl. Phys. Lett.* **2004**, 84, 2685–2687.

(16) Jackson, W. B.; Hoffman, R. L.; Herman, G. S. High-Performance Flexible Zinc Tin Oxide Field-Effect Transistors, *Appl. Phys. Lett.* **2005**, 87, 193503.

(17) Lin, Y.-H.; Faber, H.; Zhao, K.; Wang, Q.; Amassian, A.; McLachlan, M.; Anthopoulos, T. D. High-Performance ZnO Transistors Processed via an Aqueous Carbon-free Metal Oxide Precursor Route at Temperatures Between 80–180 ° C, *Adv. Mater.* **2013**, 25, 4340–4346.

(18) Jeong, J.; Pearson, C.; Lee, Y. U.; Winchester, L.; Hwang, J.; Kim, H.; Do, L. -M.; Petty, M. C. Zinc Oxide Thin Film Transistors Fabricated at Low Temperature by Chemical Spray Pyrolysis. *J. Electron. Mater.* **2014**, 43, 4241–4245.

(19) Na, J. H.; Kitamura, M.; Arakawa, Y. High Field-Effect Mobility Amorphous InGaZnO Transistors with Aluminum Electrodes, *Appl. Phys. Lett.* **2008**, 93, 063501.

(20) Kalbein, D.; Ryu, H.; Ante, F.; Fenk, B.; Hahn, K.; Kem, K.; Klauk, H. High-Performance ZnO Nanowire Transistors with Aluminum Top Gate Electrodes and Naturally Formed Hybrid Self-Assembled Monolayer-AlO_x Gate Dielectric, *ACS NANO*, **2014**, 8, 6840–6848.

(21) Lee, E.; Lee, J.; Kim, J.-H.; Lim, K.-H.; Byun, J. S.; Ko, J.; Kim, Y. D.; Park, Y.; Kim, Y. S. Direct Electron Injection into an Oxide Insulator Using a Cathode Buffer Layer, *Nat. Commun.* **2015**, 6, 6785.

(22) Ka, J.; Cho, E. N.; Lee, M.-J.; Myong, J.-M.; Yun, I. Electrode Metal Penetration of Amorphous Indium Gallium Zinc Oxide Semiconductor Thin Film Transistors, *Curr. Appl. Phys.* **2015**, 15, 675–678.

(23) Park, K.-S.; Ko, P.-S.; Kim, S.-D. Effects of N_2O Plasma Treatment on Perhydropolysilazane Spin-on-Dielectrics for Inter-Layer-Dielectric Applications. *Thin Solid Films* **2014**, 551, 57–60.

(24) Kim, S.-D.; Ko, P.-S.; Park, K.-S. Perhydropolysilazane Spin-on Dielectrics for Inter-Layer-Dielectric Applications of Sub-30 nm Silicon Technology. *Semicond. Sci. Tech.* **2013**, 28, 035008.

(25) Almeida, R. M.; Pantano, C. G. Structural Investigation of Silica Gel Films by Infrared Spectroscopy. *J. Appl. Phys.* **1990**, 68, 4225–4232.

(26) B. C. Trasferetti; R. V. Gelamo; F. P. Rouxinol; M. A. Bica de Moraes; Davanzo, C. U. Infrared Studies on Films of Carbosilazane and Siloxazane networks. *Chem. Mater.* **2005**, 17, 4685–4692.

(27) Kumaki, D.; Umeda, T.; Tokito, S. Influence of H_2O and O_2 on Threshold Voltage Shift in Organic Thin-Film Transistors: Deprotonation of SiOH on SiO_2 Gate-Insulator Surface. *Appl. Phys. Lett.* **2008**, 92, 093309.

(28) Theil, J.A.; Tsu, D. V.; Watkins, M. W.; Kim, S. S.; Lucovsky G. Local Bonding Environments of Si-OH Groups in SiO_2 Deposited by Remote Plasma-Enhanced Chemical Vapor Deposition and Incorporated by Postdeposition Exposure to Water Vapor. *J. Vac. Sci. Technol.* **1990**, 3, 1374–1381.

(29) Jang, K. S.; Wee, D.; Kim, Y. H.; Kim, J.; Ahn, T.; Ka, J. W.; Yi, M. H. Surface Modification of a Polyimide Gate Insulator with an Yttrium Oxide Interlayer for Aqueous-Solution-Processed ZnO Thin-Film Transistors. *Langmuir* **2013**, 29, 7143–7150.

(30) Chang, W.-Y.; Lai, Y.-C.; Wu, T.-B.; Wang, S.-F.; Chen, F.; Tsai, M.-J. Unipolar Resistive Switching Characteristics of ZnO Thin Films for Nonvolatile Memory Applications. *Appl. Phys. Lett.* **2008**, 92, 022110.

(31) Cross, R. B. M.; Souza, M. M. D.; Deane, S. C.; Young, N. D. A Comparison of the Performance and Stability of ZnO TFTs with Silicon Dioxide and Nitride as Gate Insulators. *IEEE Trans. Electron Dev.* **2008**, 55, 1109–1115.

(32) Tsai, T.-D.; Chang, J.-W.; Wen, T.-C.; Guo, T.-F. Manipulating the Hysteresis in Poly(vinyl alcohol)-Dielectric Organic Field-Effect Transistors toward Memory Elements. *Adv. Funct. Mater.* **2013**, 23, 4206–4214.

(33) Hwang, D. K.; Lee, K.; Kim, J. H.; Im, S.; Park, J. H.; Kim, E. Comparative Studies on the Stability of Polymer versus SiO_2 Gate Dielectrics for Pentacene Thin-Film Transistors. *Appl. Phys. Lett.* **2006**, 89, 093507.

(34) Gupta, T. Copper Interconnect Technology, Springer, 2009; p77.

(35) Sze, S. M.; Ng, K. K. Physics of Semiconductor Devices. 3rd edn. John Wiley and Sons, Inc, New York, 2007.

(36) Hamann, C.; Burghardt, H.; Frauenheim, T. Electrical Conduction Mechanisms in Solids (VFB, Berlin) 1988; p177.

(37) Chen, F.-H.; Her, J.-L.; Shao, Y.-H.; Matsuda, H.; Pan, T.-M. Structural and Electrical Characteristics of High-*k* Er_2O_3 and Er_2TiO_5 Gate Dielectrics for a-IGZO Thin-Film Transistors. *Nanoscale Research Letts*., **2013**, 8, 2–5.

(38) Kang, T. S.; Kim, T. Y.; Lee, G. M.; Sohn, H. C.; Hong, J. P. Highly Stable Solution-Processed ZnO Thin Film Transistors prepared *via* a Simple Al Evaporation Process. *J. Mat. Chem. C*. **2014**, 2, 1390–1395.

(39) Meena, J. S.; Chu, M.-C.; Chang, Y.-C.; You, H.-C.; Sing, R.; Liu P.-T.; Shieh, H.-P. D.; Chang, F.-C.; Ko, F.-H. Effect of Oxygen Plasma on the Surface States of ZnO Films used to produce Thin-Film Transistors on Soft Plastic Sheets. *J. Mat. Chem. C*. **2013**, 1, 6613–6622.

(40) Greve, D. W. Field Effect Devices and Applications: Devices for Portable, Low-Power, and Imaging Systems, 1st edn. 1998; p 87.

(41) Rha, S. H.; Jung, J.; Jung, Y.; Chung, Y. J.; Kim, U. K.; Hwang, E. S.; Park, B. K.; Park, T. J.; Choi, J.-H.; Hwang, C. S. Performance Variation according to Device Structure and the Source/Drain Metal Electrode of a-IGZO TFTs, *IEEE Trans. Electron Dev.* **2012**, 59, 3357–3363.

(42) Moffitt, C. E.; Wieliczka, D. M.; Yasuda, H. K. An XPS Study of the Elemental Enrichment on Aluminum Alloy Surfaces from Chemical Cleaning, *Surf. Coat. Technol.* **2001**, 137, 188–196.

(43) Li, H.; Belkind, A.; Jansen, F.; Orban, Z. An In Situ XPS Study of Oxygen Plasma Cleaning of Aluminum Surfaces, *Surf. Coat. Technol.* **1997**, 92, 171–177.

(44) Wang, Y.-L.; Ren, F.; Lim, W.; Norton, D. P.; Pearton, S. J.; Kravchenko, I. I.; Zavada, J. M. Room Temperature Deposited Indium Zinc Oxide Thin Film Transistors, *Appl. Phys. Lett.* **2006**, 90, 232103.

(45) Choi, W.-S. ALD-Grown ZnO Thin-Film Transistor with a Polymeric Dielectric, *J. Korean Phys. Soc.* **2009**, 53, 678–681

(46) Dehuff, N. L.; Kettenring, E. S.; Hong, D.; Chiang, H. Q.; Wager, J. F.; Hoffman, R. L.; Park, C.-H. Keszler, D. A. Transparent Thin-film Transistors with Zinc Indium Oxide Channel Layer, *J. Appl. Phys.* **2005**, 97, 064505.

(47) Jeong, S.; Kim, D.; Lee, S.; Park, B.-K.; Moon, J. Organic-Inorganic Hydrid Dielectrics with Low Leakage Current for Organic Thin-Film Transistors, *Appl. Phys. Lett.* **2006**, 89, 092101.